THREE-DIMENSIONAL, PERIODIC, 'HALO' ORBITS

KATHLEEN CONNOR HOWELL*
Stanford University, Stanford, Calif., U.S.A.

(Received 1 June, 1982; accepted 8 July, 1983)

ABSTRACT. A largely numerical study was made of families of three-dimensional, periodic, 'halo' orbits near the collinear libration points in the restricted three-body problem. Families extend from each of the libration points to the nearest primary. They appear to exist for all values of the mass ratio μ, from 0 to 1. More importantly, most of the families contain a range of stable orbits. Only near L_1, the libration point between the two primaries, are there no stable orbits for certain values of μ. In that case the stable range decreases with increasing μ, until it disappears at $\mu = 0.0573$. Near the other libration points, stable orbits exist for all mass ratios investigated between 0 and 1. In addition, the orbits increase in size with increasing μ.

1. INTRODUCTION

One of the most frequently studied models in celestial mechanics is the three-body problem. Of particular interest are the paths of motion of an infinitesimal particle under the gravitational influence of two other finite bodies. This study is concerned with motion resulting from particular initial conditions which produce periodic, three-dimensional 'halo' orbits.

Robert Farquhar coined the term 'halo' for these orbits in his Ph.D. thesis (Farquhar, 1968). In studies related to exploring the far side of the Moon (Farquhar, 1968, 1970), he found a family of three-dimensional almost periodic orbits around the equilibrium point L_2 in the Earth-Moon system - the translunar collinear libration point. At Goddard (Farquhar, 1972), Farquhar lobbied for a communications station in such an orbit for use with Apollo 18. A satellite or space station placed in this orbit has the advantage of continuous contact with both the far side of the Moon and the Earth. With control, it is never blocked from view by the Moon, thus the term 'halo'. Apollo 18 was, of course, later cancelled.

In 1973, Farquhar and Kamel (1973) used the method of Lindstedt-Poincaré to produce analytic solutions for quasi-periodic orbits about L_2.

---

* Present address: School of Aeronautics and Astronautics, Purdue University, West Lafayette, IN 47907, U.S.A.

Celestial Mechanics **32** (1984) 53-71. 0008-8714/84/0321-0053 $02.85.

Their solutions included nonlinearities, lunar orbit eccentricity and the Sun's gravitational field, all of which are hereafter ignored. The linearized motion consisted of periodic motion in the plane of the Moon's orbit, and simple harmonic motion out of the plane. For certain large values of the in-plane amplitude, a corresponding value of the out-of-plane amplitude would produce a purely periodic three-dimensional path. Farquhar and Kamel calculated some members of this halo family, all of which were unstable. The convergence of their truncated series does deteriorate, however, as orbit size increases.

A scientific satellite, the International Sun Earth Explorer (ISEE), was recently in a similar periodic halo orbit about L_1, the libration point between the Sun and Earth (Farquhar et al., 1977; Richardson, 1979). This orbit is also unstable. Station keeping costs have been modest for the ISEE satellite but could be even lower if the orbit were stable - an important consideration if applied to a large space colony in the future.

In 1979, Breakwell and Brown (1979) extended the L_2 family numerically, from the perfectly periodic orbits discovered by Farquhar and Kamel as far as almost-rectilinear orbits near the Moon. They also calculated the L_1 family as it moves toward the Moon. Both families have more out-of-plane motion and shorter periods as they approach the Moon. Of significance is the range of stable orbits found for each roughly halfway between the libration point and the Moon. Current work extends this to other mass ratios of the two finite bodies.

2. ANALYSIS

2.1. Equations of Motion

The three-body problem involves the two finite masses m_1 and m_2, assumed to be point masses, moving around their common mass center, each under the gravitational influence of the other. A rotating coordinate system, with origin at the barycenter is chosen as shown in Figure 1. μ is defined as the mass ratio m_2 to the sum m_1+m_2.

The mass ratios of some familiar systems are: Earth-Moon (0.012),

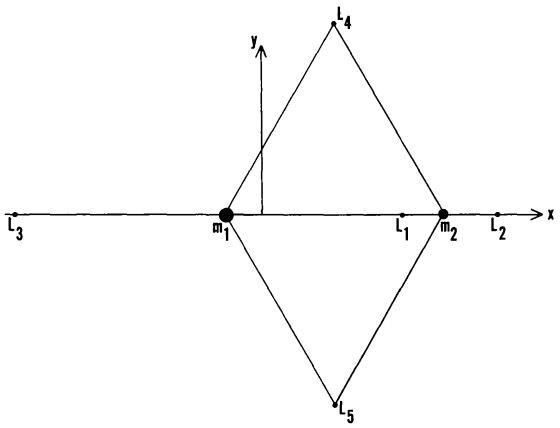

Fig. 1. Libration points in the 3-body problem.

Sun-Jupiter (9.5×10^{-4}) and Sun-Earth (3×10^{-6}). The x-y plane is the plane of motion of m_1 and m_2. A z-axis out of the paper completes the right handed system. The third body, m_3, is assumed massless but may travel in all of the three dimensions. In this system, it is well known that there are five equilibrium points, or libration points, where gravitational and centrifugal forces balance each other. Temporarily assuming $m_2<m_1$, the points are defined as shown in the figure. Of the collinear points, L_3 is defined as being on the far side of the larger mass, L_1 is between them, and L_2 on the far side of the smaller mass. As m_1 and m_2 travel around the barycenter, all five points remain in the same position relative to the masses for a given μ. For convenience, nondimensional units were chosen such that the following quantities are equal to unity: the angular velocity of the rotating frame, the distance between m_1 and m_2, and the sum of the primary masses, m_1+m_2.

The equations of motion for the system are:

$$\begin{aligned} \ddot{x} - 2\dot{y} &= \frac{\partial U}{\partial x} \\ \ddot{y} + 2\dot{x} &= \frac{\partial U}{\partial y} \\ \ddot{z} &= \frac{\partial U}{\partial z} \end{aligned} \tag{1}$$

where

$$U = \tfrac{1}{2}(x^2 + y^2) + \frac{(1-\mu)}{d_1} + \frac{\mu}{d_2};$$

$$d_1 = [(x+\mu)^2 + y^2 + z^2]^{1/2};$$

$$d_2 = [(x-1+\mu)^2 + y^2 + z^2]^{1/2};$$

$$\mu = m_2;$$

$$1-\mu = m_1.$$

This system does admit a constant of integration, the Jacobi constant, C, such that

$$C = 2U - (\dot{x}^2 + \dot{y}^2 + \dot{z}^2). \tag{2}$$

Let $\bar{X}$ be defined as the column vector $(x, y, z, \dot{x}, \dot{y}, \dot{z})^T$. Then the differential equation for the transition matrix $\Phi(t, 0)$, the matrix of partial derivatives $\partial\bar{X}(t)/\partial\bar{X}(0)$ associated with these equations of motion, is

$$\frac{d}{dt}\Phi(t, 0) = F(t)\Phi(t, 0). \tag{3}$$

F is a 6x6 matrix which is divided into 4 submatrices, each 3x3

$$F = \left(\begin{array}{c|c} 0 & I \\ \hline U_{XX} & 2\Omega \end{array}\right),$$

where

0 = zero matrix,

I = identity matrix,

$$\Omega = \begin{pmatrix} 0 & 1 & 0 \\ -1 & 0 & 0 \\ 0 & 0 & 0 \end{pmatrix},$$

And U_{XX} is the symmetric matrix of second partial derivatives of U with respect to x, y, z evaluated along the orbit. The initial condition $\Phi(0, 0)$ is equal to the identity matrix. The problem thus presents 42 first order differential equations of motion. For orbits calculated close to m_2, a time transformation from t to τ was used, such taht

$$\frac{dt}{d\tau} = d_2, \tag{4}$$

bringing the total number of differential equations to 43.

2.2. Numerical Algorithm

The following analysis closely follows Breakwell and Brown (1979). In preparing Equation (1) for integration, the initial conditions can be chosen by noting the invariance of the system under the transformation $y \rightarrow -y$ and $t \rightarrow -t$. Then the old and transformed equations will produce the same solution for the same initial conditions. The same initial conditions demand that the initial vector is

$$\bar{\underline{X}}_0 = (x_0, 0, z_0, 0, \dot{y}_0, 0)^T,$$

which is perpendicular to the x-z plane. The solution will also be symmetric with respect to the x-z plane, so if another perpendicular crossing can be found, such that

$$\bar{\underline{X}}(T/2) = (x, 0, z, 0, \dot{y}, 0)^T,$$

then the orbit will be periodic with period T.

The transition matrix at T/2 can be used to adjust the initial values of a nearby periodic orbit. Using a Kutta-Merson integration procedure, the equations are integrated until y changes sign. Then the step-size is reduced and the integration goes forward again. This is repeated, until $|y| < 10^{-11}$, and the time at this point is defined to be T/2.

The orbit is considered 'periodic' if $|\dot{x}|$ and $|\dot{z}| < 10^{-8}$ at T/2. If this is not the case, $\dot{x}$ and $\dot{z}$ can be reduced by correcting two of the three initial conditions and integrating again.

Assume $|\dot{x}|$ and $|\dot{z}|$ are too large. Let $(\delta x_0, 0, \delta z_0, 0, \delta \dot{y}_0, 0)^T$ be the corrections to the initial vector $\bar{\underline{X}}_0$. Since $y(T/2) \cong 0$ at this point, then $\delta\dot{x} = -\dot{x}$ and $\delta\dot{z} = -\dot{z}$ are the only desired changes in the end conditions. The corrections can be calculated from

$$\delta X \cong \Phi(T/2, 0)\delta X_0 + \frac{\partial X}{\partial t}\delta(T/2),$$

where

$$\delta y = 0 = \Phi_{21}\delta x_0 + \Phi_{23}\delta z_0 + \Phi_{25}\delta\dot{y}_0 + \dot{y}\delta(T/2).$$

If it is desired to change only z_0 and $\dot{y}_0$, and leave x_0 fixed, the result is

$$\begin{pmatrix}\delta\dot{x}\\ \delta\dot{z}\end{pmatrix} \simeq \left[\begin{pmatrix}\Phi_{43} & \Phi_{45}\\ \Phi_{63} & \Phi_{65}\end{pmatrix} - \frac{1}{\dot{y}}\begin{pmatrix}\ddot{x}\\ \ddot{z}\end{pmatrix}\begin{pmatrix}\Phi_{23} & \Phi_{25}\end{pmatrix}\right]\begin{pmatrix}\delta z_0\\ \delta\dot{y}_0\end{pmatrix}. \tag{5}$$

To keep z_0 fixed and change only x_0 and $\dot{y}_0$, use

$$\begin{pmatrix}\delta\dot{x}\\ \delta\dot{z}\end{pmatrix} \simeq \left[\begin{pmatrix}\Phi_{41} & \Phi_{45}\\ \Phi_{61} & \Phi_{65}\end{pmatrix} - \frac{1}{\dot{y}}\begin{pmatrix}\ddot{x}\\ \ddot{z}\end{pmatrix}\begin{pmatrix}\Phi_{21} & \Phi_{25}\end{pmatrix}\right]\begin{pmatrix}\delta x_0\\ \delta\dot{y}_0\end{pmatrix}. \tag{6}$$

Using this methodology, the convergence to a periodic halo orbit is rapid and in most cases three to four iterations are sufficient. Because the orbit is symmetric about the x-z plane, it is not necessary to calculate the second half of the orbit.

The transition matrix at the end of a complete cycle, $\Phi(T, 0)$, is needed to determine the first order stability of a given periodic orbit. Integration of the second half of the orbit to obtain $\Phi(T, 0)$ is, however, not required since $\Phi(T, 0)$ can be calculated directly from $\Phi(T/2, 0)$ which is already available. The transformation previously mentioned of $y \to -y$, $t \to -t$ is performed first. The new vector $\bar{\underline{Y}}$ can be written in terms of $\bar{\underline{X}}$ as

$$\bar{\underline{Y}} = A\bar{\underline{X}}, \tag{7}$$

where

$$A = \begin{pmatrix}1 & 0 & 0 & 0 & 0 & 0\\ 0 & -1 & 0 & 0 & 0 & 0\\ 0 & 0 & 1 & 0 & 0 & 0\\ 0 & 0 & 0 & -1 & 0 & 0\\ 0 & 0 & 0 & 0 & 1 & 0\\ 0 & 0 & 0 & 0 & 0 & -1\end{pmatrix}.$$

The new transition matrix, Ψ, is then

$$\Psi = A\Phi A. \tag{8}$$

The transformation leaves the equations of motion unchanged, so

$$\Psi(-t) = \Phi(t) \quad \text{or} \quad \Psi(T/2) = \Phi(-T/2).$$

Using relations (7) and (8) as well as the property

$$\Phi(t_2, 0) = \Phi(t_2, t_1)\Phi(t_1, 0),$$

the following can be derived:

$$\Phi(T, 0) = A\Phi^{-1}(T/2, 0)A\Phi(T/2, 0). \tag{9}$$

Now define $\Phi^* = V\Phi V^{-1}$ and note that Φ^* is symplectic, i.e., $\Phi^{*T}S\Phi^* = S$, where superscript T means transpose and

$$V = \left(\begin{array}{c|c} I & 0\\ \hline -\Omega & I\end{array}\right), \qquad S = \left(\begin{array}{c|c} 0 & I\\ \hline -I & 0\end{array}\right).$$

Then

$$\Phi^{-1}(T/2,\ 0) = V^{-1}S^{-1}V^{-T}\Phi^{T}(T/2,\ 0)V^{T}SV. \tag{10}$$

For a final result,

$$\Phi(T,\ 0) = A\left(\begin{array}{c|c} 0 & -I \\ \hline I & -2\Omega \end{array}\right)\Phi^{T}(T/2,\ 0)\left(\begin{array}{c|c} -2\Omega & I \\ \hline -I & 0 \end{array}\right)A\Phi(T/2,\ 0). \tag{11}$$

First-order stability of a particular orbit is determined by the eigenvalues of the full cycle transition matrix $\Phi(T, 0)$. For periodicity, the eigenvalues must have a modulus of 1. In addition, some observations can be made initially about the 6 eigenvalues of $\Phi(T, 0)$. First, the relation in Equation (10) shows that Φ^{-1} and Φ^{T}, or Φ, have the same eigenvalues. Second, the determinant is 1, so zero eigenvalues are excluded. Third, it can be shown that two of the eigenvalues are always 1. It may be easier and more accurate to calculate the 4 eigenvalues which are needed directly from a 4x4 matrix M:

$$\begin{pmatrix} dx \\ dz \\ d\dot{x} \\ d\dot{z} \end{pmatrix} = M\begin{pmatrix} \delta x_0 \\ \delta z_0 \\ \delta\dot{x}_0 \\ \delta\dot{z}_0 \end{pmatrix}. \tag{12}$$

since it is shown that $\delta y = \delta y_0 = 0$. To determine an expression for M, start with the following total derivative:

$$\begin{pmatrix} dx \\ dy \\ dz \\ d\dot{x} \\ d\dot{y} \\ d\dot{z} \end{pmatrix} = \Phi\begin{pmatrix} \delta x_0 \\ \delta y_0 \\ \delta z_0 \\ \delta\dot{x}_0 \\ \delta\dot{y}_0 \\ \delta\dot{z}_0 \end{pmatrix} + \begin{pmatrix} \dot{x} \\ \dot{y} \\ \dot{z} \\ \ddot{x} \\ \ddot{y} \\ \ddot{z} \end{pmatrix}\delta(T/2). \tag{13}$$

Assume x_0, z_0, $\dot{x}_0$, $\dot{z}_0$ vary so that the Jacobi constant, C, from Equation (2) remains constant. The derivative of (2), evaluated at t = 0, produces $\delta\dot{y}_0$ as a function of δx_0 and δz_0, since

$$\frac{\partial C}{\partial \dot{y}_0}\delta\dot{y}_0 + \frac{\partial C}{\partial x_0}\delta x_0 + \frac{\partial C}{\partial z_0}\delta z_0 = 0,$$

with only three nonzero terms. $\delta(T/2)$ can also be expressed as a function, then, of δx_0, δz_0, $\delta\dot{x}_0$, $\delta\dot{z}_0$ by using the second of the Equations in (13)

$$dy = 0 = \Phi_{21}\delta x_0 + \Phi_{23}\delta z_0 + \Phi_{24}\delta\dot{x}_0 + \Phi_{25}\delta\dot{y}_0 + \Phi_{26}\delta\dot{z}_0 + \dot{y}\delta(T/2).$$

The resulting M matrix is

$$M = \begin{pmatrix} \Phi_{11} & \Phi_{13} & \Phi_{14} & \Phi_{16} \\ \Phi_{31} & \Phi_{33} & \Phi_{34} & \Phi_{36} \\ \Phi_{41} & \Phi_{43} & \Phi_{44} & \Phi_{46} \\ \Phi_{61} & \Phi_{63} & \Phi_{64} & \Phi_{66} \end{pmatrix} - \frac{1}{\partial C/\partial\dot{y}_0}\begin{pmatrix} \Phi_{15} \\ \Phi_{35} \\ \Phi_{45} \\ \Phi_{65} \end{pmatrix}\begin{pmatrix} \frac{\partial C}{\partial x_0} & \frac{\partial C}{\partial z_0} & 0 & 0 \end{pmatrix} -$$

$$-\frac{1}{\dot{y}}\begin{pmatrix}0\\0\\\ddot{x}\\\ddot{z}\end{pmatrix}\left[(\Phi_{21}\quad \Phi_{23}\quad \Phi_{24}\quad \Phi_{26}) \quad -\frac{\Phi_{25}}{\partial C/\partial \dot{y}_0}\left(\frac{\partial C}{\partial x_0}\quad \frac{\partial C}{\partial z_0}\quad 0\quad 0\right)\right].$$

The eigenvalues determined from M will be the reciprocal pairs λ_1, $1/\lambda_1$, λ_2, $1/\lambda_2$. A solution will be periodic only if the modulus of λ is equal to 1. Since complex λ will be accompanied by its conjugate, all λ must be on the unit circle for stability. To more easily show results, two stability indices have been defined.

$$\nu_i = \tfrac{1}{2}(\lambda_i + 1/\lambda_i), \quad i = 1, 2.$$

For a given orbit, stability is indicated if

$$|\nu_i| \leq 1, \quad i = 1, 2,$$

and ν_i is real.

3. RESULTS

Approximately 1000 orbits were calculated to produce the following results. This number was necessary because a reasonable initial guess for an orbit was derived from the initial conditions of a previous solution. The study was started by using values obtained by Breakwell and Brown in the Earth-Moon case ($\mu \tilde{=} 0.012$).

3.1. The L_1 Halo Family

Shown in Figures 2a-c are members of the L_1 family at μ=0.04. Table I contains the initial conditions (x_0, z_0, $\dot{y}_0$) and final values for some of

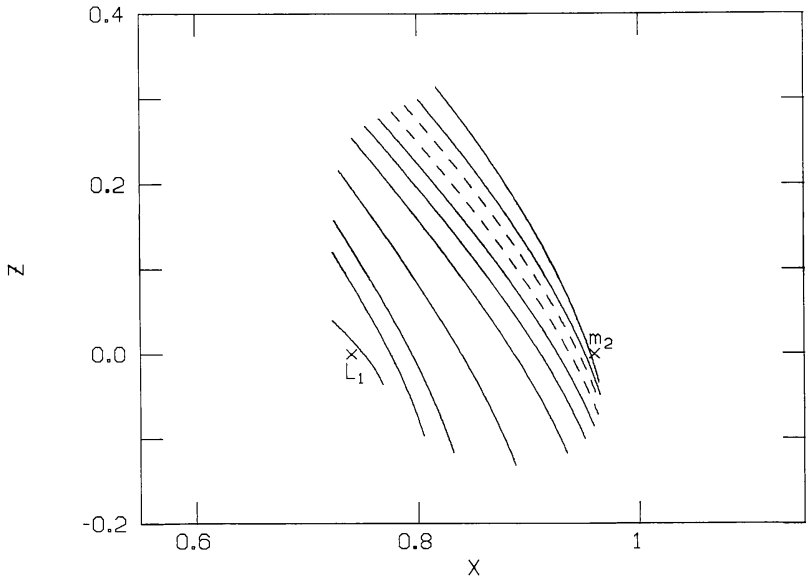

Fig. 2a. X-Z projection, L_1 family, μ=0.04.

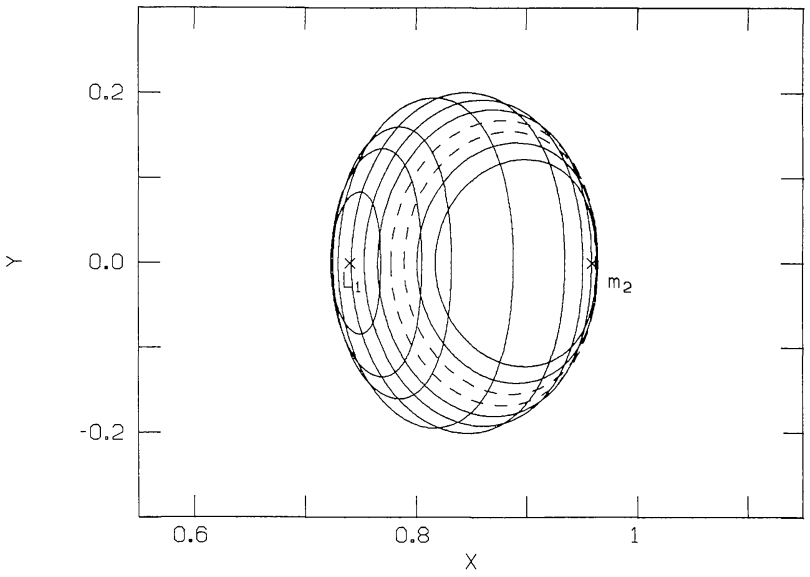

Fig. 2b. X-Y projection, L_1 family, μ=0.04.

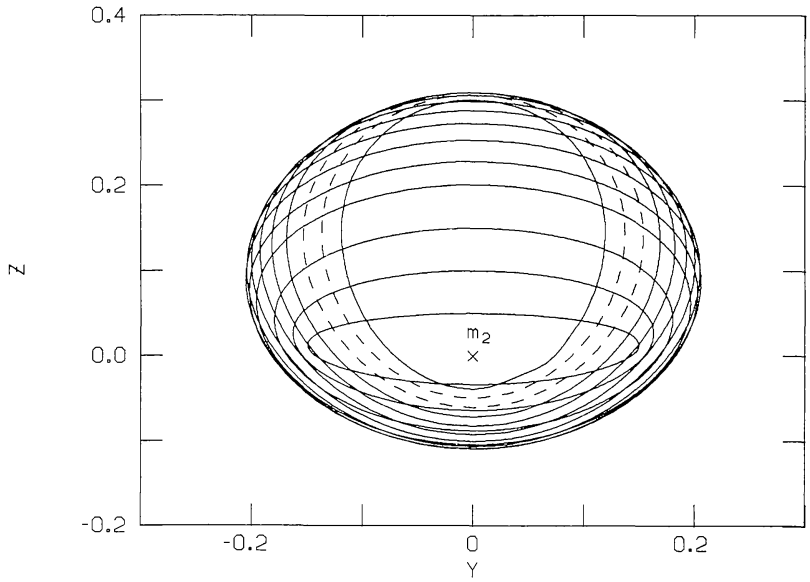

Fig. 2c. Y-Z projection, L_1 family, μ=0.04.

the orbits shown in the figures. In Table I, recall that x_0 is defined from the barycenter, T/2 is the number of nondimensional time units in half the period for the given orbit. C is the Jacobi constant from Equation (2), and ν_1 and ν_2 are the stability indices. In the figures is the northern family. In all cases a mirror-image southern family can be obtained by reversing the sign of z. Note the small size of the orbits. The period is decreasing as the move closer to m_2. Work done by Breakwell and Brown suggests that even closer to the mass than those shown, the orbits get larger with increasing z values and longer in period. The region of stable orbits is bounded by the dashed orbits seen in the figures. It is located

in Table I between the orbits with values x_0=0.729988 and x_0=0.801125.

To study the stability, each orbit in the family is designated by its minimum x value. The maximum z value also occurs at this point which was used as the starting point in the numerical integration. Using these as identifying points for each orbit, the stability indices for μ=0.04 are shown in Figure 3. Recall that ν_1 and ν_2 are calculated from the eigen-

TABLE I: Initial conditions for L_1 family at μ=0.04.

x_0	0.723268	0.729988	0.753700	0.777413	0.801125	0.817724
z_0	0.040000	0.215589	0.267595	0.284268	0.299382	0.313788
$\dot{y}_0$	0.198019	0.397259	0.399909	0.361870	0.312474	0.271306
T/2	1.300177	1.348532	1.211253	1.101099	1.017241	0.978635
C	3.329168	3.030033	2.937178	2.928754	2.930700	2.929481
ν_1	1181.69	51.07839	4.95816	1.101843	0.94834	1.10361
ν_2	0.98085	-0.90203	-0.40587	-0.420200	-1.58429	-2.09182

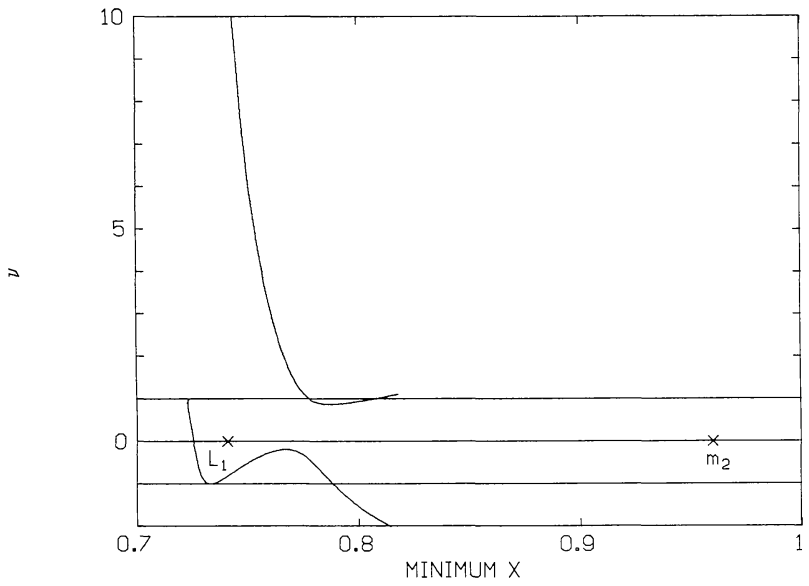

Fig. 3. Stability indices, L_1 family, μ=0.04.

values of the M matrix and that both must be between -1 and +1 for stability. The region of stable orbits indicated earlier is seen to exist. For the orbits closer to m_2 but not shown, the stability indices return to $|\nu_i| \leq 1$ but they are near-collision orbits and were not of interest in this study. Figure 4 uses the stability curves at various mass ratios and shows only the parts of the curves at or near the 'middle' stable zone. All curves have been normalized such that the distance of L_1 to m_2 is equal.

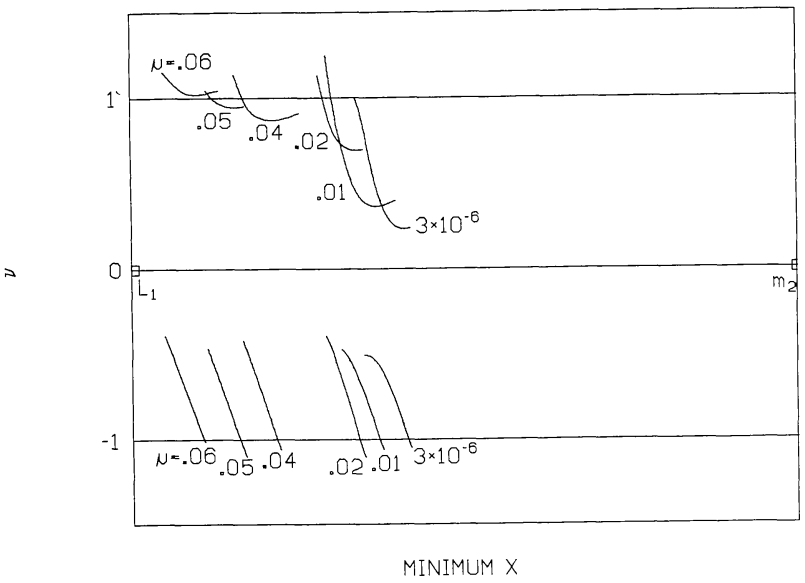

Fig. 4. Stability indices, L_1 families.

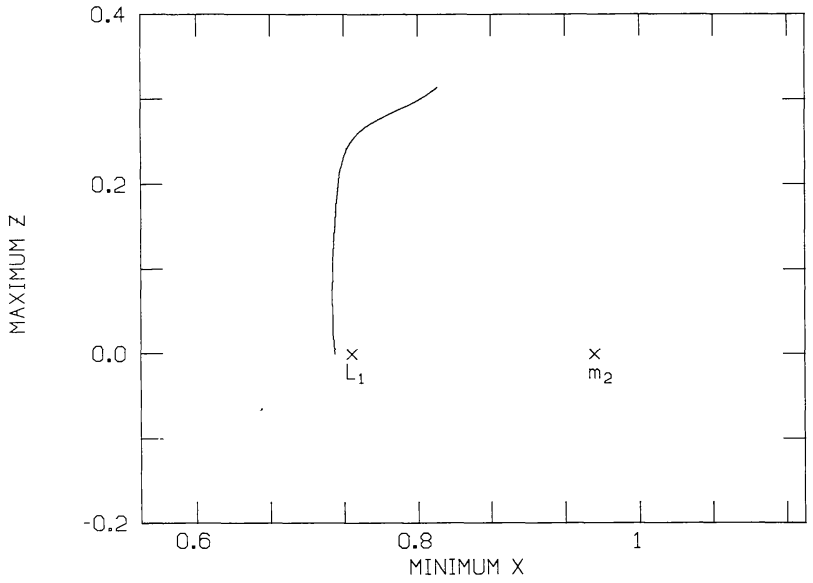

Fig. 5. X-Z profile, L_1 family, μ=0.04.

The top values, ν_1, define the boundary of the stable range of orbits near L_1. The bottom values, ν_2, define the boundary near m_2. Increasing the mass ratio moves the curves close to L_1, but also increases ν_1. ν_1 fails to dip below +1 when $\mu \tilde{=} 0.0573$. Other families at higher mass ratios were not pursued. The curves labelled μ=0.001 was done for a system containing primary masses equal to the Sun and Jupiter. The curve $\mu = 3 \times 10^{-6}$ represents the Sun-Earth system.

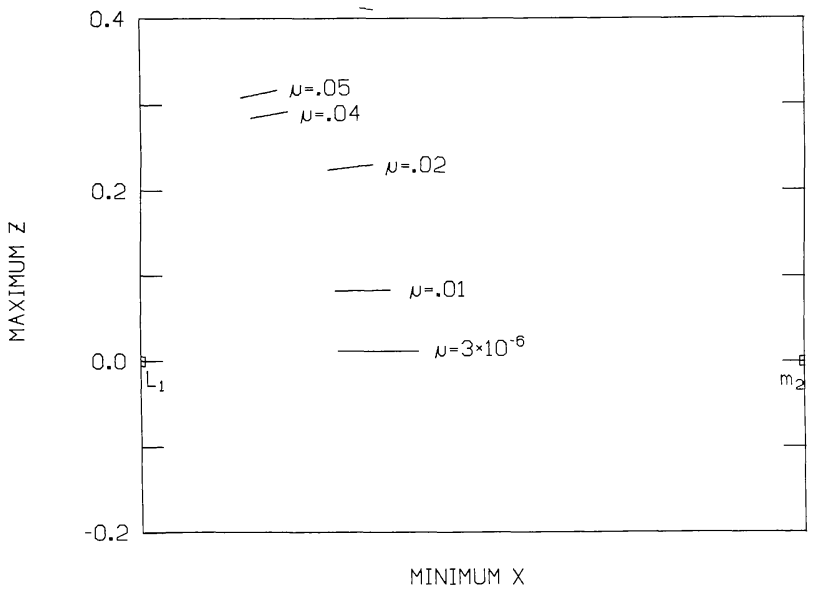

Fig. 6. Stable regions, L_1 families.

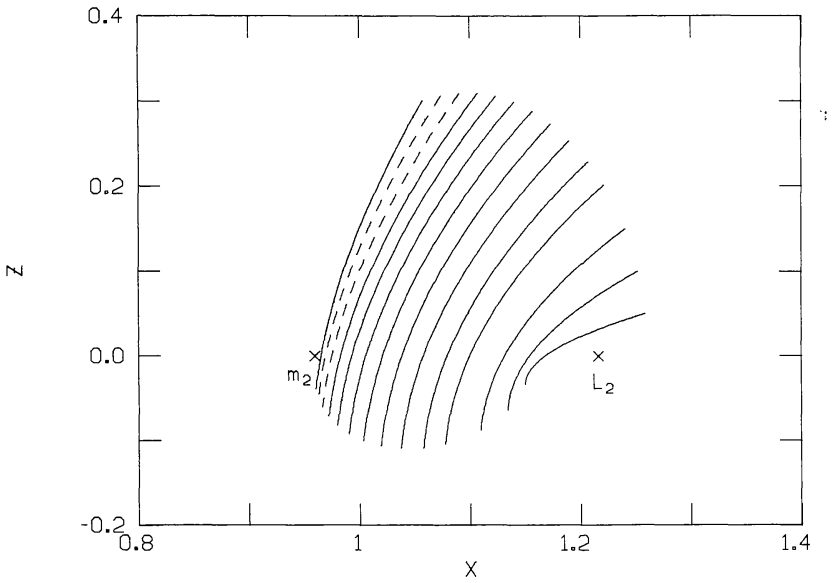

Fig. 7a. X-Z projection, L_2 family, μ=0.04.

The effects of mass ratio can also be studied by using plots like Figure 5. Using x_{min} for orbit identification, a curve plotting x_{min} versus the corresponding z_{max} values is presented for the μ=0.04 family. It is seen to be the left boundary of the x-z projection in Figure 2a. A similar profile can be drawn for each mass ratio. In Figure 6, only the parts of those profiles whose orbits fall in the stable zone have been drawn. Again, the curves have been normalized so the L_1 to m_2 distance is equal. Increasing μ moves the stable zone closer to the libration point. It also increases the out-of-plane motion, thus making the orbits larger. The size of the zone appears to be decreasing, however.

3.2. The L_2 Halo Family

The families originating near the equilibrium point L_2 are more interesting because the stable halos continue to exist for all values of μ tested. The projections of this family at μ=0.04 are shown in Figures 7a-c. The initial conditions for some of these orbits are contained in Table II. As before, the stable range is bounded by dashed orbits. In the table these are contained within the range from x_0=1.057222 to x_0=1.140216. The size of all the orbits is comparable to those near L_1. Somewhat similar to L_1, the period of the orbits increases as x_0 moves away from m_2.

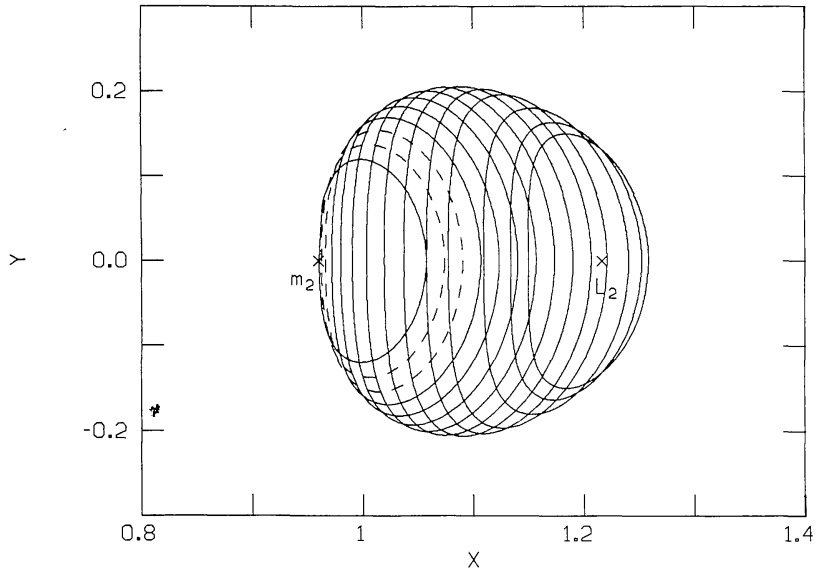

Fig. 7b. X-Y projection, L_2 family, μ=0.04.

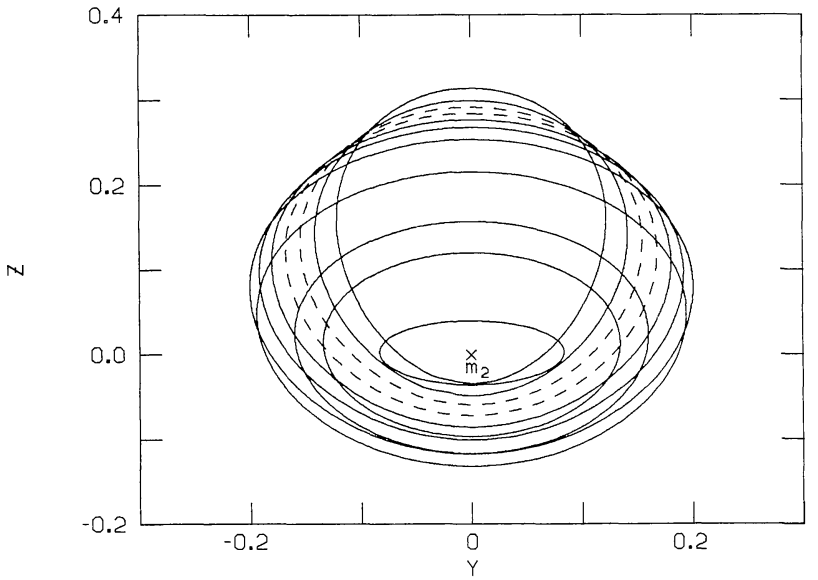

Fig. 7c. Y-Z projection, L_2 family, μ=0.04.

TABLE II: Initial conditions for L_2 family at μ=0.04.

x_0	1.057222	1.092791	1.140216	1.173414	1.220839	1.258203
z_0	0.300720	0.309254	0.298898	0.272900	0.200987	0.050000
$\dot{y}_0$	-0.238026	-0.281140	-0.316028	-0.324710	-0.310434	-0.250410
T/2	1.019032	1.205930	1.433655	1.562199	1.700458	1.791154
C	3.001826	2.987945	3.006462	3.046136	3.140834	3.262822
ν_1	-0.01038	0.61156	11.54674	35.36097	143.9507	458.2081
ν_2	-1.43755	-0.71170	-0.98759	-0.61975	0.38028	0.98301

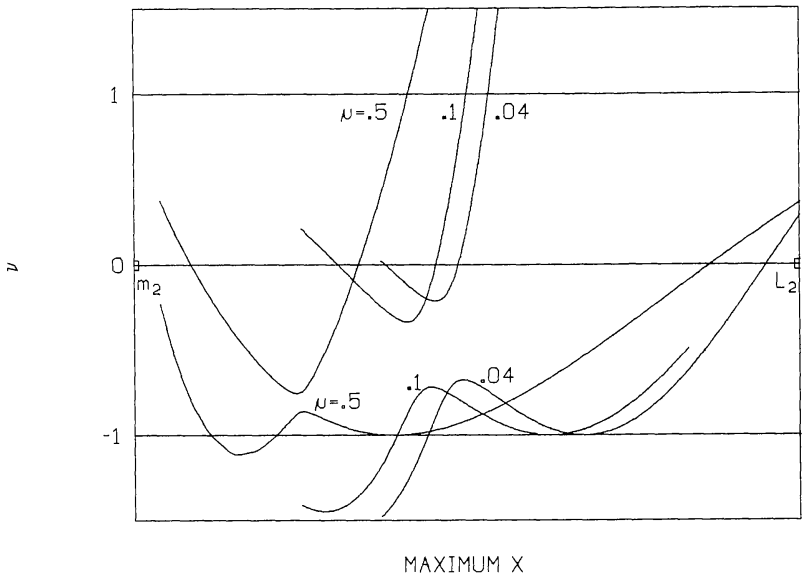

Fig. 8. Stability indices, L_2 families.

Since L_2 is on the far side of m_2, orbits in this family are designated by their maximum x value, as seen in Figure 7a. Again, this point corresponds to the maximum z value and was the initial point for integration. Unlike L_1, however, calculating orbits with values of x_{max} less than those shown, would produce decreasing values of z_{max}.

Some values of ν_1 amd ν_2 can be seen in Figure 8. The position of each orbit defined by its x_{max} value is plotted versus its stability indices. The scale is again chosen so that the m_2 to L_2 distance is equal for all curves. The 'middle' stable region of interest, where $|\nu_i| \leq 1$, is roughly halfway between m_2 and L_2. It is defined on the right near L_2 by ν_1, the upper value. It is defined near the mass, m_2, on the left by ν_2. The plot also shows in the case of μ=0.5, that near to m_2, ν_2 returns to the stable zone. This, in fact, happens at all the mass ratios. As in the L_1 family, they become near-collision, almost rectilinear orbits and were not initially considered. Orbits in the region have generated new interest since Figure 8

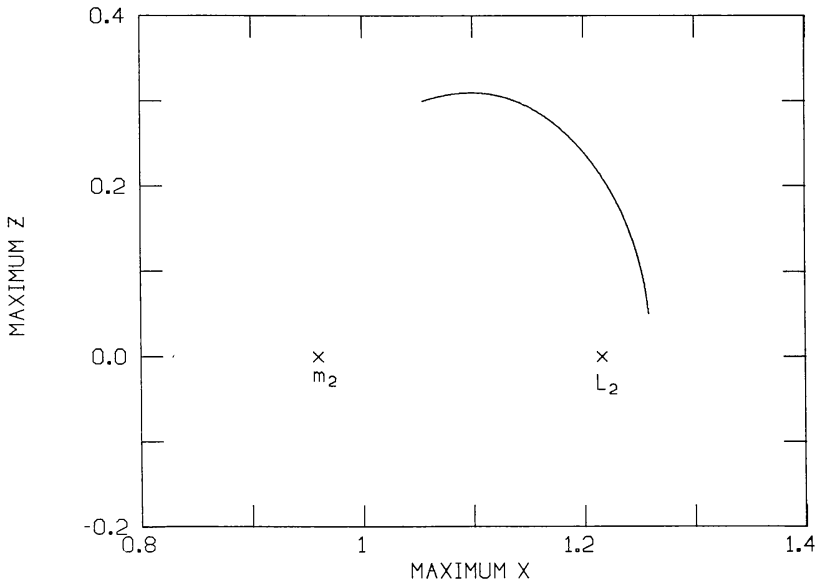

Fig. 9. X-Z profile, L_2 family, μ=0.04.

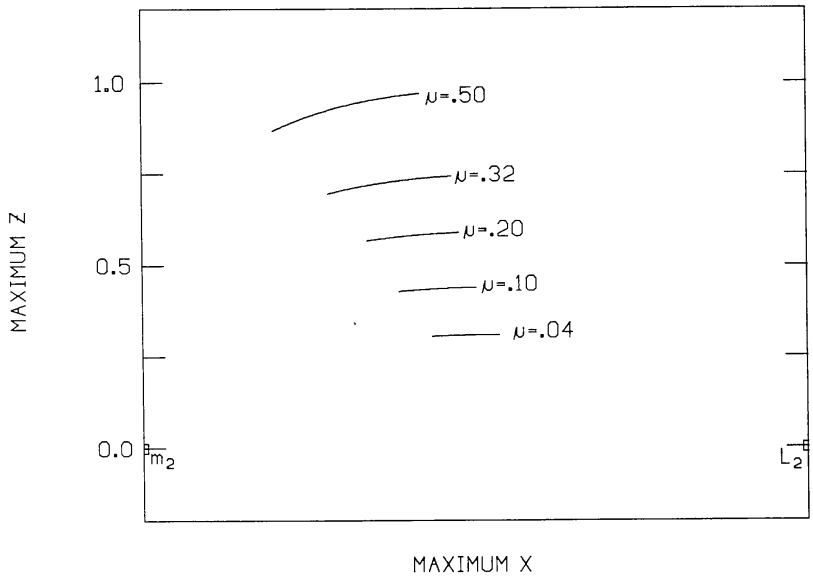

Fig. 10. Stable regions, L_2 families.

indicates that for μ>0.5 the two regions of stability may merge. This possibility is explored further in the next section.

The locus of initial points of the μ=0.04 L_2 family is shown in Figure 9. A corresponding curve can be drawn for other mass ratios. Figure 10 uses the parts of those profiles, scaled appropriately, which include stable orbits. The increasing size of the stable zone with μ is apparent. As was the case with L_1, the large values of μ have more out-of-

plane motion as well. The orbits at μ=0.5 are quite a bit larger than those at μ=0.04. At μ=0.05, the z_{max} values are almost 4 times the values of μ=0.04. In contrast to L_1, these stable solutions are moving closer to the mass m_2 rather than the libration point.

3.3. The L_3 Halo Family

In the three-body problem, the libration point on the far side of the larger mass is defined to be L_3. Therefore, when μ is greater than 0.5, the point to its right in Figure 1, which has been labelled L_2, is now L_3. This, of course, means that now $m_2 > m_1$. However, the mass ratio is still defined $\mu=m_2/(m_1+m_2)$. All the conditions present in the L_2 families still hold, and the same trends continue. L_3 families can be viewed as the extension of those near L_2 for μ approaching 1.

TABLE III: Initial conditions for L_3 family at μ=0.96.

x_0	0.268434	0.528350	0.801947	1.212341	1.485937	1.670940
z_0	1.812789	1.797900	1.675254	1.311769	0.869490	0.100000
$\dot{y}_0$	-0.194347	-0.391878	-0.598423	-0.904561	-1.108238	-1.246284
T/2	2.801110	2.953177	3.010512	3.049978	3.063561	3.069570
C	1.121650	1.190433	1.361169	1.774411	2.148595	2.444230
ν_1	0.99740	1.31950	1.51942	1.82300	2.14123	2.419349
ν_2	0.74492	0.91490	0.95994	0.98686	0.99596	0.99995

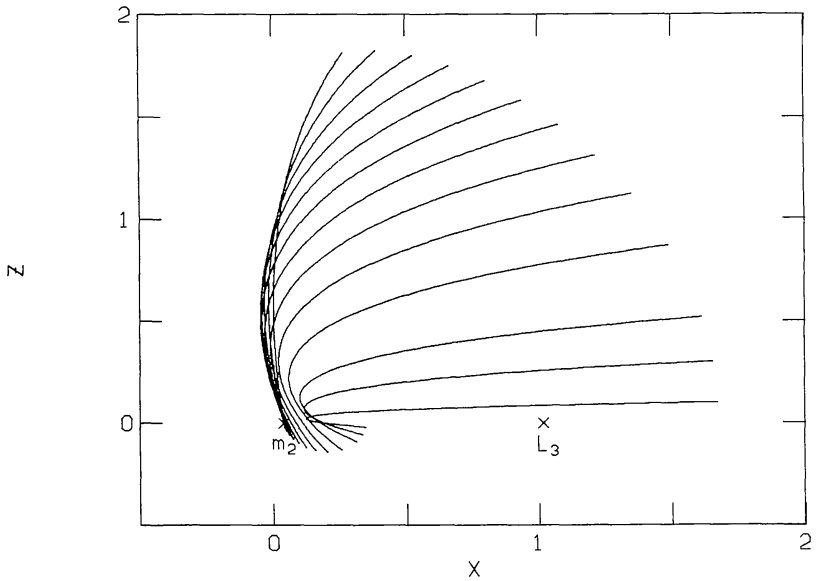

Fig. 11a. X-Z projection, L_3 family, μ=0.96.

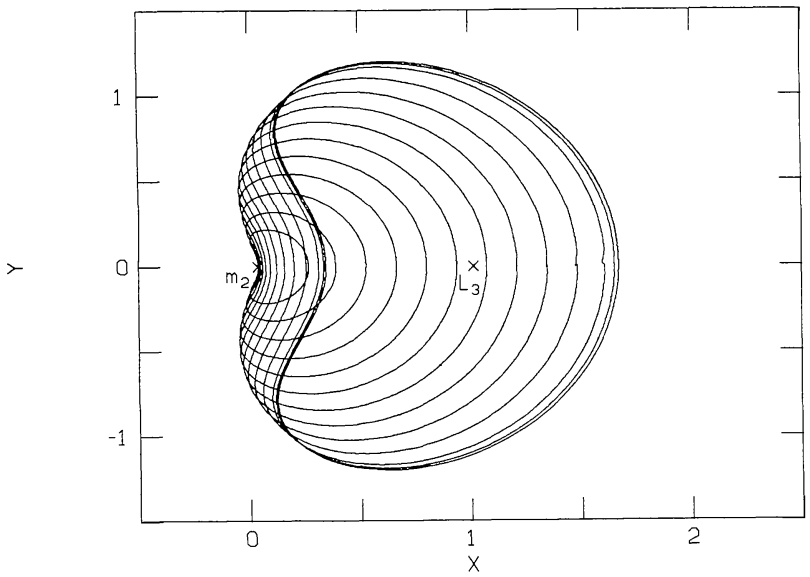

Fig. 11b. X-Y projection, L_3 family, μ=0.96.

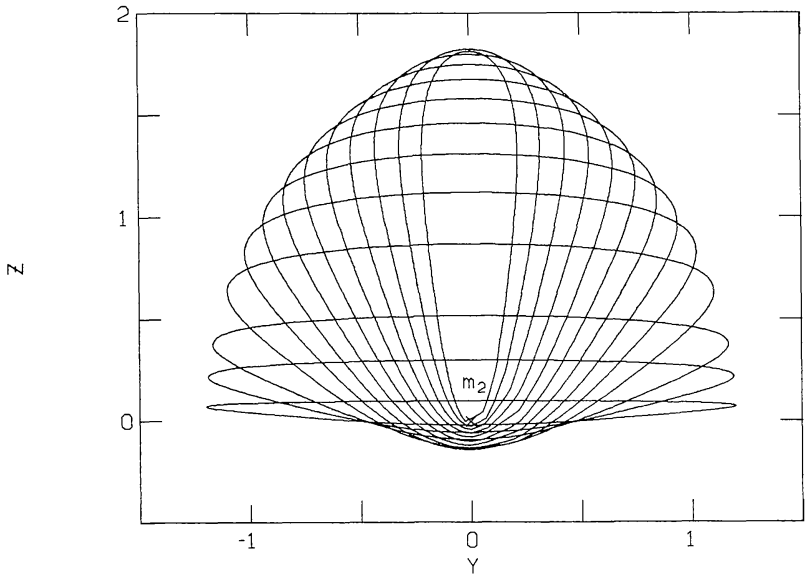

Fig. 11c. Y-Z projection, L_3 family, μ=0.96.

The L_3 family μ=0.96 is the completion of the case where the smaller mass has the value 0.04. The projections of the orbits in this family appear in Figures 2 and 7. Some of the corresponding initial conditions are shown in Table III. These orbits are much larger than those shown in Figures 2 and 7. In the case μ=0.96, the members of th L_3 family have dimensions at least 5 times the size of corresponding orbits in the L_1 and L_2 families. As they approach the mass the orbits grow very long and thin and the period

decreases, although only slightly. These projections show no dashed orbits used previously to indicate stability. The orbit shown with x_{max} closest to m_2 in Figure 11a, is actually just on the edge of a stable region.

Figure 12 shows the values of ν_1 and ν_2 for three mass ratios. Clearly the stability indices return to the stable zone near m_2. The figure adds support to a possible merger of the 'middle' stable zone and the region close to the mass. A mass ratio of 0.80 is the highest value at which two

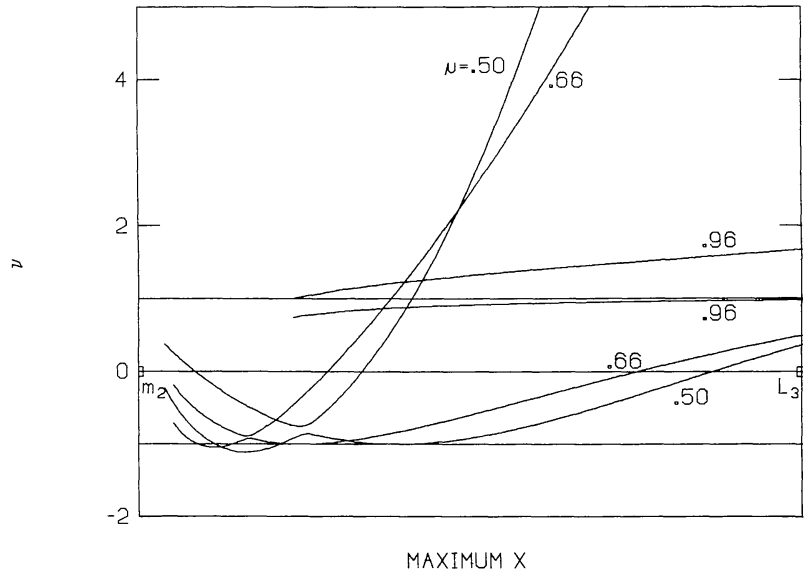

Fig. 12. Stability indices, L_3 families.

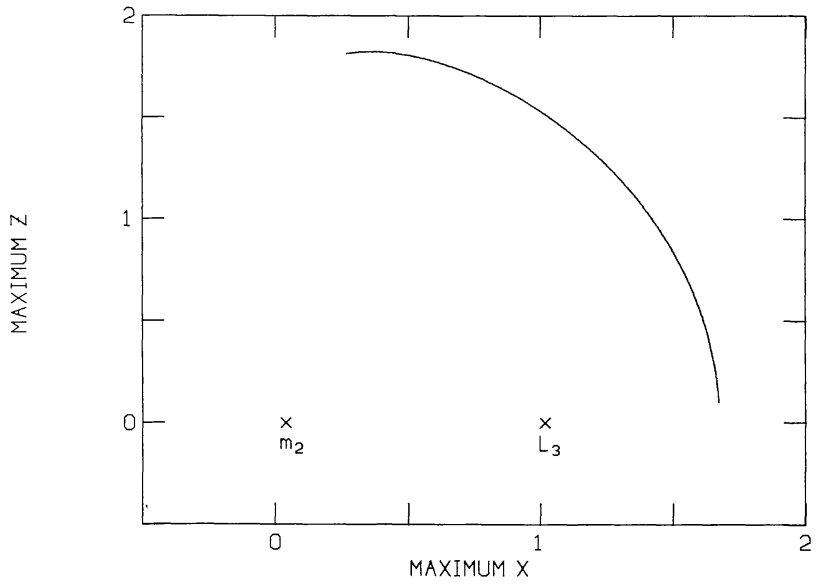

Fig. 13. X-Z profile, L_3 family, μ=0.96.

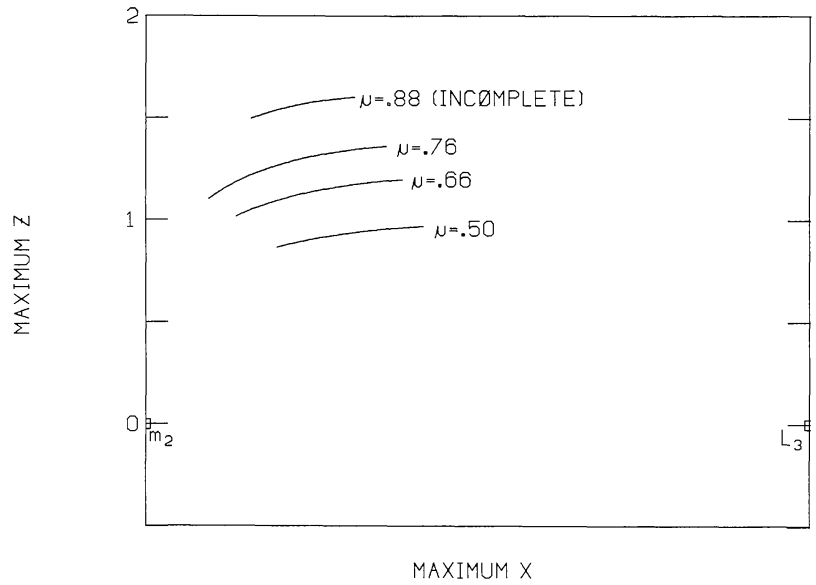

Fig. 14. Stable regions, L_3 families.

separate regions of stability could be calculated. The case μ=0.96 shows the large change in appearance of curves ν_1 and ν_2. Although dramatic in the figure, it does happen gradually as μ grows. ν_1 for μ=0.96 is very close to dipping below +1, showing that solution to be on the edge of stability. Further members of this family could not be produced because of numerical difficulties encountered in calculating the orbits any closer to m_2 at that value of μ. These orbits are becoming long, thin and near collision, which is causing the numerical problems.

Figure 13 is the locus of initial points for μ=0.96. No point here is actually stable, but the point nearest m_2 is bordering the region. Parts of other such curves at different mass ratios in the important 'middle' stable region are shown in Figure 14. (The curve for μ=0.5 is, of course, the same for both L_2 and L_3.) Figure 14 shows again an increase in out-of-plane motion and an increase in size of the stable range consistent with results in the L_2 case. The curve μ= 0.88 is marked incomplete because of the numerical difficulties encountered. The z_{max} values and the right boundary of the stable range can be noted though for μ=0.88.

4. CONCLUSIONS AND FUTURE WORK

Halo orbits exist near all three collinear libration points at a wide range of mass ratios. Near L_1 and L_2 they are comparable in size for a given mass ratio, and increase in size as μ increases. As a continuation of the L_2 families, the orbits near L_3 continue to grow in size with μ. For a given small value of the smaller mass, the L_3 family may be an order of magnitude larger than those at L_1 and L_2. Most orbits decrease in period as they approach the nearest mass. Stable orbits exist roughly halfway between each

each libration point and its nearest mass. Near L_1, the stable orbits move closer to the libration point with increasing μ until they disappear at $\mu \cong 0.0573$. Near L_2 and L_3, this 'middle' stable range moves closer to the nearest mass. At high mass ratios near L_3, it may possible merge with another stable zone of near collision orbits.

The numerical difficulties encountered have delayed answers to questions arising during the study. Currently, a regularizing program is being written which will produce solutions as distance from m_2 approaches zero, as well as indicate the stability of those solutions. More investigations of the L_3 family may also include μ=0.988, which represents the Earth-Moon case.

REFERENCES

Breakwell, J. V. and Brown, J. V.: 1979, 'The "Halo" Family of 3-Dimensional Periodic Orbits in the Earth-Moon Restricted 3-Body Problem', Celest. Mech. 20, 389.

Farquhar, R. W.: 1968, 'The Control and Use of Libration-Point Satellites', Ph.D. Dissertation, Dept. of Aeronautics and Astronautics, Stanford University, Stanford, Calif., U.S.A.

Farquhar, R. W.: 1970, 'The Control and Use of Libration-Point Satellites', NASA TR R-346.

Farquhar, R. W.: 1972, 'A Halo-Orbit Lunar Station', Astronautics and Aeronautics, pp. 59-63.

Farquhar, R. W. and Kamel, A. A.: 1973, 'Quasi-Periodic Orbits About the Translunar Libration Point', Celest. Mech. 7, 458.

Farquhar, R. W., Muhonen, D. P., and Richardson, D. L.: 1977, 'Mission Design for a Halo Orbiter of the Earth', J. Spacecraft Rockets 14, 170.

Richardson, D. L.: 1979, 'Halo-Orbit Formulation for the ISEE-3 Mission', AAS Paper, 79-127.